HHS Public Access

Author manuscript

Nat Med. Author manuscript; available in PMC 2013 August 09.

Published in final edited form as:

Nat Med. 2012 November ; 18(11): 1693–1698. doi:10.1038/nm.2960.

PKCθ Regulates T-Cell Leukemia-Initiating Activity via Reactive Oxygen Species

Vincenzo Giambra[1], **Christopher R. Jenkins**[1], **Hongfang Wang**[2], **Sonya H. Lam**[1], **Olena O. Shevchuk**[1], **Oksana Nemirovsky**[1], **Carol Wai**[1], **Sam Gusscott**[1], **Mark Y. Chiang**[3], **Jon C. Aster**[2], **R. Keith Humphries**[1], **Connie Eaves**[1], and **Andrew P. Weng**[1]

[1]Terry Fox Laboratory, BC Cancer Agency, Vancouver, BC V5Z 1L3, Canada

[2]Department of Pathology, Brigham & Women's Hospital/Harvard Medical School, Boston, MA 02115, USA

[3]Division of Hematology/Oncology, University of Michigan Cancer Center, Ann Arbor, MI 48103, USA

Abstract

Reactive oxygen species (ROS), a by-product of cellular metabolism, damage intracellular macromolecules and, in excess, can promote normal hematopoietic stem cell differentiation and exhaustion[1–3]. However, mechanisms that regulate ROS levels in leukemia-initiating cells (LICs) and the biological role of ROS in these cells remain largely unknown. We show here the ROS^{low} subset of $CD44^{+}$ cells in T-cell acute lymphoblastic leukemia (T-ALL), a malignancy of immature T-cell progenitors, to be highly enriched in the most aggressive LICs, and that ROS are maintained at low levels by downregulation of protein kinase C theta (PKCθ). Strikingly, primary mouse T-ALLs lacking PKCθ show improved LIC activity whereas enforced PKCθ expression in both mouse and human primary T-ALLs compromised LIC activity. We also demonstrate that PKCθ is positively regulated by RUNX1, and that NOTCH1, which is frequently activated by mutation in T-ALL[4–6] and required for LIC activity in both mouse and human models[7,8], downregulates PKCθ and ROS via a novel pathway involving induction of RUNX3 and subsequent repression of RUNX1. These results reveal key functional roles for PKCθ and ROS in T-ALL and suggest that aggressive biological behavior in vivo could be limited by therapeutic strategies that promote PKCθ expression/activity or ROS accumulation.

Current therapies for T-ALL achieve cure in 80% of pediatric cases, but only 40% of adults survive beyond 5 years[9]. The ineffectiveness of chemotherapeutic regimens in both age groups may be attributed to an inability to target LICs[10–12] which exhibit relative quiescence, resistance to apoptosis, expression of DNA repair enzymes and drug efflux

Correspondence: Andrew P. Weng, MD, PhD, BC Cancer Agency, 675 West 10th Avenue (CRC 12-111), Vancouver, BC V5Z 1L3 Canada, aweng@bccrc.ca, tel: 604-675-8136, fax: 604-877-0712.

The authors declare no competing financial interests.

V.G. and A.P.W designed the experiments; V.G., C.R.J., S.H.L., O.O.S., O.N., C.W., and S.G. generated the data; V.G. and A.P.W. interpreted the results; M.Y.C. provided reagents and advice; H.W. and J.C.A. generated and analyzed ChIP-Seq data; R.K.H. and C.E. provided advice and discussion; and V.G. and A.P.W. wrote the paper.

pumps, and localization within protective/inaccessible niches[13]. More efficient targeting of LICs could thus lead to dramatic improvements in patient outcomes.

Much recent interest has focused on the role of reactive oxygen species (ROS) in normal and malignant stem cell biology[14]. ROS are chemically-reactive molecules that participate in self-propagating reactions, and if allowed to accumulate, can cause oxidative damage to intracellular macromolecules including DNA, proteins, and lipids[15,16]. Normal hematopoietic stem cells are uniquely sensitive to ROS[1–3], and some cancer stem cells that exhibit low ROS levels lose stem activity or become non-viable when ROS levels are increased[17,18].

To address the role of ROS in T-ALL, we focused first on LICs in a well-defined mouse model in which animals are reconstituted with syngeneic bone marrow cells transduced with constitutively activated NOTCH1-ΔE retrovirus. This approach produces aggressive, serially transplantable T-cell leukemias within 8–12 weeks that are highly similar to human T-ALL[19–21]. Transplantation of primary NOTCH1-ΔE leukemia cells at limiting dilution into secondary recipients revealed the LIC frequency to be 1 in ~6,100 total cells (Fig. 1a). Using the cell-permeable indicator dye DCFDA to assess intracellular ROS levels[22] in combination with various surface markers, we noted that the $CD44^+$ fraction contains a subset of cells with low ROS (Fig. 1b). To determine if LIC activity was asymmetrically distributed within this subpopulation, $CD44^+ROS^{low}$, $CD44^+ROS^{high}$, and $CD44^-$ subsets were prospectively isolated by FACS and injected into immunocompetent syngeneic (C57BL/6) and immunocompromised NOD/Scid/*Il2rg*$^{-/-}$ (NSG) recipients. Interestingly, the $CD44^+ROS^{low}$ fraction showed substantially enriched LIC activity as compared to complementary $CD44^+ROS^{high}$ and $CD44^-$ fractions (Fig. 1c and Supplementary Fig. 1), and recapitulated the original tumor heterogeneity (Supplementary Fig 2). Similar findings were observed in a second T-ALL model initiated by K-ras^{G12D} (Fig. 1d), indicating that enriched LIC activity within the $CD44^+ROS^{low}$ fraction is not confined to the NOTCH1 model.

To assess the relevance of these findings to human disease, we transplanted FACS-sorted ROS^{high} vs. ROS^{low} subsets of human T-ALL samples into NSG recipients. These samples had previously been expanded in NSG mice[20] to obtain sufficient material for replicate studies. CD44 was not included in the LIC sorting strategy because most of the xenograft-expanded human samples in our collection already contain high percentages of $CD44^+$ cells (data not shown). Consistent with our observations in mouse models, LIC activity was enriched in the ROS^{low} fraction in human leukemias (Fig. 1e). Taken together, these studies show that LICs in both mouse and human T-ALL are characterized by low levels of ROS.

PKCθ is a critical signaling intermediate downstream of the T-cell receptor (TCR)/preTCR[23,24] and is activated in T-ALLs arising in Notch3-IC transgenic mice[23]. PKCθ has also been implicated in ROS production in normal T cells[25]. To explore whether PKCθ might be involved in regulating ROS levels in T-ALL cells, we first surveyed PKCθ expression in the NOTCH1-ΔE mouse model. We noted PKCθ protein levels to vary among primary leukemias (Fig. 2a) and that levels of PKCθ and ROS were correlated (Fig. 2b). Moreover, T-ALLs generated from PKCθ^{null} bone marrow[24] had very low ROS levels, and

that restoration of PKCθ expression by retroviral transduction significantly increased ROS (Fig. 2c). A survey of human T-ALL cell lines and xenograft-expanded human T-ALL samples also revealed varying levels of PKCθ protein (Fig. 2d). Of note, retroviral PKCθ expression in HPBALL cells (with low endogenous PKCθ) increased ROS, whereas shRNA-mediated PKCθ knock-down in RPMI 8402 cells (with high endogenous PKCθ) decreased ROS (Fig. 2e,f and Supplementary Fig. 3a,b). Taken together, these data support a dominant role for PKCθ in regulating ROS levels in both mouse and human T-ALL.

We next asked whether low ROS that characterizes LIC-enriched fractions might be due to reduced PKCθ expression. Indeed, LIC-enriched $CD44^+$ and $CD44^+ROS^{low}$ fractions from mouse leukemias exhibited significantly less PKCθ mRNA and protein than corresponding LIC-depleted $CD44^-$ and $CD44^+ROS^{high}$ fractions, respectively (Fig. 2g,h and Supplementary Fig. 3c,d). Similarly, LIC-enriched ROS^{low} fractions of human leukemias showed significantly less PKCθ than corresponding LIC-depleted ROS^{high} fractions (Fig. 2i,j and Supplementary Fig. 3e). These data suggest that varied expression of PKCθ contributes to heterogeneous ROS levels and LIC activities in subpopulations of T-ALL cells.

To address directly the role of PKCθ in regulating LIC activity, competitive transplants were performed between $PKC\theta^{null}$ and wild-type leukemias, the latter with either high or low levels of endogenous PKCθ. In each case, recipient mice developed leukemias composed predominantly of $PKC\theta^{null}$ cells (Supplementary Fig. 4a). Of note, a minor population of $PKC\theta^{low}$ cells was detected in some recipients of $PKC\theta^{null}$ vs. $PKC\theta^{low}$ cells, as might be expected if increasing PKCθ "dose" progressively compromised LIC activity. Competitive transplants were also performed between isogenic $PKC\theta^{RV}$ ($PKC\theta^{null}$ cells transduced with retroviral PKCθ) and parental $PKC\theta^{null}$ cells. In recipient mice, resulting leukemias were composed nearly entirely of $PKC\theta^{null}$ cells, consistent with enforced PKCθ expression having compromised LIC activity (Fig. 3a,b). Importantly, $PKC\theta^{RV}$ cells produced leukemia under non-competitive transplant conditions, excluding a non-specific toxic effect of enforced PKCθ expression. Strikingly, lentiviral expression of a constitutively activated form of $PKC\theta^{26}$ in xenograft-expanded human T-ALL cells abrogated LIC activity (Fig. 3c and Supplementary Fig. 4b), again supporting the idea that increasing PKCθ "dose" has increasingly dramatic negative effects on LIC activity.

The frequency of LICs in $PKC\theta^{null}$ and wild-type leukemias was very similar, indicating that reduced PKCθ is permissive to, but not sufficient for LIC activity (Supplementary Fig. 5). Of note, $PKC\theta^{null}$ and wild-type leukemias exhibit similar latencies in both primary and secondary transplant assays, and PKCθ overexpression or knock-down does not affect cell proliferation, suggesting that proliferation or other measures of aggressiveness cannot explain why leukemias with lower PKCθ levels prevail *in vivo*. Rather, these data support the idea that PKCθ has a dominant role in determining the ability of T-ALL cells to reconstitute/initiate disease *in vivo*. Of note, low PKCθ levels were also associated with resistance to chemotherapy and radiation (Supplementary Fig. 6) which might also confer aggressive behavior in patients.

To explore how PKCθ expression is regulated in T-ALL, we examined available microarray data and discovered that the transcription factor RUNX1, recently described as a tumor suppressor in T-ALL[27–29], was highly correlated with PKCθ in four separate patient cohorts totaling 264 primary samples[30–33] (Fig. 4a and Supplementary Fig. 7). ChIP-Seq for RUNX1 in the NOTCH1-mutated human T-ALL cell line CUTLL1[34] revealed four high confidence RUNX1 binding sites within the PKCθ locus, one located at the proximal promoter (associated with H3K4me3 chromatin marks) and three within putative intronic enhancers (associated with H3K4me1 chromatin marks)[35] (Fig. 4b), suggesting that RUNX1 might regulate PKCθ expression. Consistent with this idea, shRNA-mediated knock-down of RUNX1 resulted in decreased PKCθ mRNA and protein (Fig. 4c,d). Interestingly, ChIP-Seq for NOTCH1 in the same cells[36] revealed two high confidence NOTCH1/CSL binding sites located 30–60 kb upstream of the RUNX3 P1 promoter[37] and associated with H3K4me1 chromatin marks (Fig. 4e), suggesting that NOTCH1 might regulate RUNX3 expression. Combined with the notion that RUNX proteins can activate or repress target gene expression[38], we hypothesized that a transcriptional circuit might be active in T-ALL cells in which NOTCH1 activates RUNX3, RUNX3 represses RUNX1, and RUNX1 activates PKCθ (Fig. 4f). In fact, RUNX3 overexpression or knock-down resulted in reciprocal changes in RUNX1 expression, while blocking NOTCH1 by treating cells with γ-secretase inhibitor (GSI) decreased RUNX3, increased RUNX1, and increased PKCθ (Fig. 4g,h and Supplementary Fig. 8). Dominant negative Mastermind-like-1 (DN-MAML)[39] recapitulated GSI effects on RUNX3, confirming that these effects are specific to NOTCH signaling. Furthermore, GSI treatment caused ROS levels to increase, a response that did not occur in PKCθ^{null} mouse leukemias and which was abrogated by PKCθ inhibition or RUNX1 knock-down in human T-ALL cells (Fig. 4i and Supplementary Fig. 8). These results thus reveal a novel mechanism connecting NOTCH1 to LIC activity though negative regulation of PKCθ and ROS levels, and are consistent with prior studies showing that Notch signaling promotes LIC activity[7,8]. Variation among individual cell lines suggests other factors likely impinge upon components of the NOTCH1-RUNX3-RUNX1-PKCθ transcriptional circuit; however, the overall consistent effects support the relevance of these results.

Our findings suggest that PKCθ may play a broad role in regulating LIC activity in T-ALL. While the identified pathway linking NOTCH1 and PKCθ is likely most relevant in cases with activating NOTCH1[6] or inactivating FBW7[4,5] mutations, PKCθ expression may be similarly reduced in cases with RUNX1 mutation/loss-of-function (recently reported to occur in 4–18% of cases[27–29]) or elevated RUNX3 expression, or by NOTCH/RUNX-independent mechanisms. Alternatively, cell signaling events that modulate PKCθ activity rather than expression level per se[40] may also have important effects on LIC activity. Further studies will be required to explore the intriguing possibility that therapies which promote PKCθ expression and/or activity may antagonize LICs and thereby improve clinical outcomes in patients with T-ALL.

Online Methods

Mice

PKCθ (*Prkcq*) knock-out mice (backcrossed over 10 generations to C57BL/6) have been described previously[24]. We obtained C57BL/6 (Ly5.2), B6.SJL-Ptprc^{a}Pepc^{b}/BoyJ (Ly5.1), and NOD/Scid/*Il2rg*$^{-/-}$ (NSG) mice from in-house colonies maintained at the BC Cancer Agency (BCCA) Animal Resource Centre. We housed all animals in specific pathogen-free facilities according to institutional guidelines. All breeding and animal experiments were performed under protocols approved by the University of British Columbia (UBC) Animal Care Committee and according to guidelines of the Canadian Council on Animal Care.

Viruses

We produced high titer, replication-defective retroviral supernatants by transient transfection of PlatE cells[41], and lentivirus by transient co-transfection of 293T cells with packaging/envelope vectors as described[42]. MSCV-based retroviral expression vectors encoding constitutively active NOTCH1 (ΔE or L1601P-ΔPEST alleles) with IRES-GFP or IRES-tNGFR cassettes for tagging of transduced cells have been described[19,21,39]. We constructed similar retroviral expression vectors carrying a wild-type PKCθ cDNA. The dominant negative Mastermind-like-1 (DN-MAML) retroviral construct encoding amino acids 13–74 of human MAML1 fused to GFP has been previously described[39]. We expressed RUNX3 and constitutively activated PKCθ (A148E mutation)[26] cDNAs from the lentiviral vector pRRL-cPPT/CTS-MNDU3-PGK-GFP-WPRE which is composed of the pRRLsin-18 backbone[43,44], cPPT with central DNA flap[45,46], MNDU3 promoter[47,48], PGK-GFP marker, and WPRE element (plasmid construction details available upon request). We cloned the RNAi Consortium (TRC) shRNAs[49] targeting PKCθ (shPKCθ-91, TRCN0000001791; shPKCθ-92, TRCN0000001792), RUNX1 (shRUNX1-58, TRCN0000013658; shRUNX1-59, TRCN0000013659), and RUNX3 (shRUNX3, TRCN0000235674) into pLKO.1puro lentivector as described[50]. We obtained the scrambled shRNA control (shScramble) in pLKO.1puro vector from Addgene (#1864)[51]. We verified all constructs by sequencing. We isolated virally transduced cells by fluorescence activated cell sorting (FACS) or by selection with puromycin as applicable.

Bone Marrow Transplantation

To generate primary mouse leukemias, we transduced bone marrow cells from 5-fluorouracil treated mice (C57BL/6 background) with retrovirus by spinoculation[20]. Three days later, we injected 10,000–40,000 GFP^{+} or NGFR^{+} cells (including at least 1×10^{5} normal bone marrow cells) into the tail vein of lethally irradiated (810 rad) C57BL/6 recipients. For serial transplantation experiments, we injected varying numbers of total or FACS-sorted primary leukemia cells by tail vein into non-irradiated C57BL/6 or sublethally irradiated (200 rad) NSG secondary recipient mice. We monitored all transplant recipient mice daily for clinical signs of leukemia. We also followed leukemia engraftment and progression in some recipients by periodic peripheral blood sampling and flow cytometric analysis.

Human Samples

We obtained all human samples with appropriate institutional approvals (UBC/BCCA Research Ethics Board, Institutional Review Board of the Institut Universitaire d'Hématologie/Université Paris Diderot, Karmanos Cancer Center Institutional Review Board, and MD Anderson Cancer Center Institutional Review Board) and informed consent under guidelines established by the Declaration of Helsinki. We isolated mononuclear cells from fresh bone marrow aspirate or peripheral blood samples by density gradient centrifugation and used them directly or cryopreserved them. Subsequent analyses utilized human-specific antibodies against CD45, CD3, CD4, and/or CD8 (eBioscience) to discern human T-ALL blasts.

Cell Culture

All established cell lines have been reported previously[6,34,52]. We cultured these cell lines in RPMI 1640 medium supplemented with 10% fetal calf serum, 1 mM sodium pyruvate, 2 mM L-glutamine, and antibiotics. We isolated primary mouse leukemia cells from the bone marrow or spleen of moribund mice and, where indicated, cultured them briefly *in vitro* in complete media as above with supplemental cytokines IL-2 and IL-7, each at 10 ng ml^{-1} (Peprotech). We expanded primary human T-ALL lymphoblasts as xenografts in sublethally irradiated in NSG mice and, where indicated, cultured them briefly *in vitro* on MS5/MS5-DL1 feeders[7] or immobilized Ig-DL1 ligand[53] as described[20].

To inhibit PKCθ enzymatic activity, we treated cells *in vitro* with 5 μM myristoylated PKCθ pseudosubstrate inhibitor (cat #539636, Calbiochem). To inhibit Notch signaling, we treated cells *in vitro* with 1 μM γ-secretase inhibitor XXI (compound E; cat #ALX-270-415, Alexis). To reduce ROS levels directly, we treated cells *in vitro* with the vitamin E-derivative antioxidant, Trolox (Calbiochem) at 50 μM final concentration.

We achieved doxycycline-inducible expression of DN-MAML[39] by lentiviral transduction of cells with pLVX-Tet-On Advanced (Clontech, CMV-IE promoter replaced with EF1α promoter) followed by selection in G418, then with DN-MAML in pLVX-Tight-Puro (Clontech) followed by selection in puromycin.

Chemotherapy and Radiation Resistance Assays

To assess drug sensitivity *in vitro*, we treated cells with doxorubicin (5 μg ml^{-1} for primary mouse leukemias, 2 μg ml^{-1} for human cell lines) or dexamethasone (10 μg ml^{-1} for primary mouse leukemias, 100 μg ml^{-1} for human cell lines) and assayed 48–72 hours later. To assess radiation sensitivity *in vitro*, we treated cells with X-irradiation using a single 10 Gy dose and assayed 48–72 hours later. We measured cell viability by flow cytometry for exclusion of propidium iodide. To assess DNA damage *in vitro*, we treated cells with X-irradiation using a single 1 Gy dose, cultured them for 1 hour, and then analyzed them for phospho-histone H2A.X by flow cytometry.

Flow Cytometry

We stained mouse and human leukemia cells with fluorochrome or biotin-conjugated antibodies against CD45, CD3, CD4, CD8, and CD44 (eBioscience, Biolegend). We used

anti-hCD271 (1:50 dilution; cat #130-091, Miltenyi Biotec) to detect the retroviral NGFR marker. We performed intracellular staining with antibodies against PKCθ (1:5 dilution; cat #560216, BD Biosciences), RUNX3 (1:40 dilution; cat #MAB3765, R&D Systems), and phospho-histone H2A.X (Ser139) (1:50 dilution; cat #9718, Cell Signaling) after paraformaldehyde fixation and permeabilization with 90% ice-cold methanol (for PKCθ and H2A.X) or saponin (for RUNX3) as specified by the manufacturer. Where applicable, we also used fluorchrome-conjugated secondary antibodies (1:100 dilution, Biolegend). To assess ROS levels, we stained live cells with 5-(and-6)-carboxy-2',7'-dichlorodihydrofluorescein diacetate (carboxy-H_2-DCFDA), dihydroethidine (DHE), or Mitosox according to the manufacturer's instructions (Invitrogen). We measured cell proliferation by BrdU incorporation according to the manufacturer's instructions (BrdU kit, BD Biosciences). We measured cell viability by propidium iodide exclusion. We performed FACS analysis and sorting on FACS Calibur, Canto2, Vantage DiVa, and Aria2 cytometers (BD Biosciences). We analyzed flow cytometry data using FlowJo software (TreeStar).

Quantitative PCR

We extracted total RNA after cell lysis in Trizol reagent (Invitrogen). We generated first strand cDNA by reverse transcription with SuperScript III (Invitrogen) using a mix of random 15-mer and anchored oligo(dT) primers, then amplified product by quantitative real-time PCR using Platinum SYBR Green qPCR SuperMix-UDG (Invitrogen) and a Bio-Rad Chromo4 optical detector. Specific primer sequences are available upon request. We assayed each sample in triplicate and calculated expression levels by the ΔΔCt method with normalization to β-actin.

Western Blot and Immunofluorescence

To generate whole cell lysates, we washed cells in ice-cold phosphate-buffered saline, then lysed them in ice-cold 50 mM Tris-HCl (pH 7.4), 1% Nonidet P-40, 0.25% sodium deoxycholate, 150 mM sodium chloride, 1 mM sodium orthovanadate, 1 mM sodium fluoride, 2.5 mM sodium pyrophosphate, 1 mM EDTA, 1 mM phenylmethylsulfonyl fluoride, and protease inhibitor cocktail (1:500 dilution; cat #539134, Calbiochem). We ran whole cell lysates on SDS-PAGE gels and then transferred them to Hybond-ECL membranes (Amersham). We blocked membranes with 5% nonfat dry milk, then probed with primary antibodies against PKCθ (1:500 dilution; cat #2059, Cell Signaling), RUNX1 (1:1,000 dilution; cat #39000, Active Motif), RUNX3 (1:1,000 dilution; cat #MAB3765, R&D), ERK2 (1:1,000 dilution; cat #sc-154, Santa Cruz), β-actin (1:6,000 dilution; cat #A1978, Sigma), and tubulin (1:5,000 dilution; cat #MAB3408, Chemicon). We used HRP-conjugated secondary antibodies (1:5,000–1:10,000 dilution; Jackson ImmunoLaboratories) with enhanced chemiluminescence (cat #32106, Pierce) and detected signals by autoradiography. We quantified band intensities using ImageJ software[54].

We performed immunofluorescence on formaldehyde-fixed, methanol-permeabilized cells from cytospin preparations using PKCθ primary antibody (1:25 dilution; cat #2059, Cell Signaling) followed by AlexaFluor 488-conjugated goat anti-rabbit secondary antibody (1:100 dilution; cat #A-11008, Invitrogen) and DAPI counterstaining. We acquired images using a Zeiss Axioplan fluorescence microscope with 20X and 40X objectives.

ChIP-Seq

We performed chromatin immunoprecipitation (ChIP) with the ChIP Assay kit (Millipore). Briefly, we treated cells with 1% formaldehyde for 10 minutes at 37 °C, lysed them in 1% SDS, 10 mM EDTA, 50mM Tris (pH 8.1), and sonicated them to obtain DNA fragments from 200–600bp. We then immunoprecipitated chromatin with the following antibodies: RUNX1 (cat #ab23980, Abcam), Notch1 (Tc)[55], CSL (kind gift of Dr. Elliott Kieff), H3K4me1 (cat #ab8895, Abcam), H3K4me3 (cat #07-745, Millipore), and H3K27me3 (cat #07-449, Millipore). Following overnight incubation with antisera at 4 °C, we captured immunoprecipitated chromatin with Protein A-agarose beads which we subsequently washed and eluted bound chromatin. After reversal of cross-links, we purified DNA using the QIAquick PCR purification kit (Qiagen). We prepared ChIP-Seq libraries according to the Illumina ChIP DNA library preparation kit. Following addition of adaptors, we amplified libraries by 18 cycles of PCR, size selected (150–250 bp) by electrophoresis, and purified using a Qiagen gel extraction kit. Following quality control testing on an Agilent 2100 Bioanalyzer, we subjected the library to deep sequencing using an Illumina Genome Analyzer II in the Harvard Medical School Biopolymers Core facility. We aligned sequencing reads to human genome build hg19 and analyzed using CisGenome[56]. Mapped reads ranged from 1×10^7 to 3.4×10^7 per library.

Microarray Data Analysis

We downloaded normalized datasets from the Gene Expression Omnibus (http://www.ncbi.nlm.nih.gov/geo/) and analyzed them using dChip software[57].

Statistics

We analyzed quantitative data using GraphPad Prism 5 software. We calculated LIC frequencies from limiting dilution transplant results as described[58].

Supplementary Material

Refer to Web version on PubMed Central for supplementary material.

Acknowledgements

We would like to thank Z. Sun (City of Hope, Duarte, CA) for providing PKCθ knock-out mice, J. Fletcher and W. Ou (Brigham & Women's Hospital, Boston, MA) for PKCθ shRNA lentivectors, E. Martignani for help with immunofluorescence, I. Bernstein (Fred Hutchinson Cancer Research Center, Seattle, WA) for Ig-DL1 ligand, F. Pflumio (Commissariat à l'énergie Atomique Fontenay-aux-Roses, France) for providing the MS5-DL1 cell line and "M" series patient T-ALL samples, L. Matherly (Karmanos Cancer Institute, Detroit, MI) for providing the "D" series patient T-ALL samples, and M.J. You (MD Anderson Cancer Center, Houston, TX) for providing the "H" series patient T-ALL samples. This work was supported by grants from the Canadian Institutes of Health Research/Terry Fox Foundation, Leukemia & Lymphoma Society of Canada, Cancer Research Society, Lymphoma Foundation Canada (to A.P.W), and the US National Cancer Institute (P01CA119070 to J.C.A). M.Y.C. was supported by a career development award from the US National Cancer Institute (K08CA120544). A.P.W. was a Michael Smith Foundation for Health Research Scholar.

References

1. Ito K, et al. Reactive oxygen species act through p38 MAPK to limit the lifespan of hematopoietic stem cells. Nat Med. 2006; 12:446–451. [PubMed: 16565722]

2. Owusu-Ansah E, Banerjee U. Reactive oxygen species prime Drosophila haematopoietic progenitors for differentiation. Nature. 2009; 461:537–541. [PubMed: 19727075]
3. Tothova Z, et al. FoxOs are critical mediators of hematopoietic stem cell resistance to physiologic oxidative stress. Cell. 2007; 128:325–339. [PubMed: 17254970]
4. O'Neil J, et al. FBW7 mutations in leukemic cells mediate NOTCH pathway activation and resistance to {gamma}-secretase inhibitors. J. Exp. Med. 2007; 204:1813–1824. [PubMed: 17646409]
5. Thompson BJ, et al. The SCFFBW7 ubiquitin ligase complex as a tumor suppressor in T cell leukemia. The Journal of Experimental Medicine. 2007; 204:1825–1835. [PubMed: 17646408]
6. Weng AP, et al. Activating Mutations of NOTCH1 in Human T Cell Acute Lymphoblastic Leukemia. Science. 2004; 306:269–271. [PubMed: 15472075]
7. Armstrong F, et al. NOTCH is a key regulator of human T-cell acute leukemia initiating cell activity. Blood. 2009; 113:1730–1740. [PubMed: 18984862]
8. Tatarek J, et al. Notch1 inhibition targets the leukemia-initiating cells in a Tal1/Lmo2 mouse model of T-ALL. Blood. 2011
9. Pui CH, Evans WE. Treatment of acute lymphoblastic leukemia. N Engl J Med. 2006; 354:166–178. [PubMed: 16407512]
10. Cox CV, et al. Characterization of a progenitor cell population in childhood T-cell acute lymphoblastic leukemia. Blood. 2007; 109:674–682. [PubMed: 17003368]
11. Gerby B, et al. Expression of CD34 and CD7 on human T-cell acute lymphoblastic leukemia discriminates functionally heterogeneous cell populations. Leukemia. 2011; 25:1249–1258. [PubMed: 21566655]
12. Chiu PP, Jiang H, Dick JE. Leukemia-initiating cells in human T-lymphoblastic leukemia exhibit glucocorticoid resistance. Blood. 2010; 116:5268–5279. [PubMed: 20810926]
13. Reya T, Morrison SJ, Clarke MF, Weissman IL. Stem cells, cancer, and cancer stem cells. Nature. 2001; 414:105–111. [PubMed: 11689955]
14. Kobayashi CI, Suda T. Regulation of reactive oxygen species in stem cells and cancer stem cells. Journal of Cellular Physiology. 2012; 227:421–430. [PubMed: 21448925]
15. Valko M, et al. Free radicals and antioxidants in normal physiological functions and human disease. The International Journal of Biochemistry & Cell Biology. 2007; 39:44–84. [PubMed: 16978905]
16. Adly AAM. Oxidative Stress and Disease: An Updated Review. Res. J. Immunol. 2010; 3:129–145.
17. Guzman ML, et al. The sesquiterpene lactone parthenolide induces apoptosis of human acute myelogenous leukemia stem and progenitor cells. Blood. 2005; 105:4163–4169. [PubMed: 15687234]
18. Diehn M, et al. Association of reactive oxygen species levels and radioresistance in cancer stem cells. Nature. 2009; 458:780–783. [PubMed: 19194462]
19. Chiang MY, et al. Leukemia-associated NOTCH1 alleles are weak tumor initiators but accelerate K-ras-initiated leukemia. J Clin Invest. 2008; 118:3181–3194. [PubMed: 18677410]
20. Medyouf H, et al. Acute T-cell leukemias remain dependent on Notch signaling despite PTEN and INK4A/ARF loss. Blood. 2010; 115:1175–1184. [PubMed: 20008304]
21. Pear WS, et al. Exclusive development of T cell neoplasms in mice transplanted with bone marrow expressing activated Notch alleles. J. Exp. Med. 1996; 183:2283–2291. [PubMed: 8642337]
22. Eruslanov E, Kusmartsev S. Identification of ROS using oxidized DCFDA and flowcytometry. Methods Mol Biol. 2010; 594:57–72. [PubMed: 20072909]
23. Felli MP, et al. PKC[theta] mediates pre-TCR signaling and contributes to Notch3- induced T-cell leukemia. Oncogene. 2004; 24:992–1000. [PubMed: 15592506]
24. Sun Z, et al. PKC-theta is required for TCR-induced NF-kappaB activation in mature but not immature T lymphocytes. Nature. 2000; 404:402–407. [PubMed: 10746729]
25. Kaminski M, Kiessling M, Suss D, Krammer PH, Gulow K. Novel role for mitochondria: protein kinase Ctheta-dependent oxidative signaling organelles in activation-induced T-cell death. Mol Cell Biol. 2007; 27:3625–3639. [PubMed: 17339328]

26. LeHoux JG, Dupuis G, Lefebvre A. Control of CYP11B2 Gene Expression through Differential Regulation of Its Promoter by Atypical and Conventional Protein Kinase C Isoforms. Journal of Biological Chemistry. 2001; 276:8021–8028. [PubMed: 11115506]
27. Della Gatta G, et al. Reverse engineering of TLX oncogenic transcriptional networks identifies RUNX1 as tumor suppressor in T-ALL. Nat Med. 2012
28. Grossmann V, et al. Prognostic relevance of RUNX1 mutations in T-cell acute lymphoblastic leukemia. Haematologica. 2011
29. Zhang J, et al. The genetic basis of early T-cell precursor acute lymphoblastic leukaemia. Nature. 2012; 481:157–163. [PubMed: 22237106]
30. Coustan-Smith E, et al. Early T-cell precursor leukaemia: a subtype of very high-risk acute lymphoblastic leukaemia. The Lancet Oncology. 2009; 10:147–156. [PubMed: 19147408]
31. Gutierrez A, et al. The BCL11B tumor suppressor is mutated across the major molecular subtypes of T-cell acute lymphoblastic leukemia. Blood. 2011; 118:4169–4173. [PubMed: 21878675]
32. Homminga I, et al. Integrated Transcript and Genome Analyses Reveal NKX2-1 and MEF2C as Potential Oncogenes in T Cell Acute Lymphoblastic Leukemia. Cancer Cell. 2011; 19:484–497. [PubMed: 21481790]
33. Winter SS, et al. Identification of genomic classifiers that distinguish induction failure in T-lineage acute lymphoblastic leukemia: a report from the Children's Oncology Group. Blood. 2007; 110:1429–1438. [PubMed: 17495134]
34. Palomero T, et al. CUTLL1, a novel human T-cell lymphoma cell line with t(7;9) rearrangement, aberrant NOTCH1 activation and high sensitivity to [gamma]-secretase inhibitors. Leukemia. 2006; 20:1279–1287. [PubMed: 16688224]
35. Heintzman ND, et al. Distinct and predictive chromatin signatures of transcriptional promoters and enhancers in the human genome. Nat Genet. 2007; 39:311–318. [PubMed: 17277777]
36. Burns CE, Traver D, Mayhall E, Shepard JL, Zon LI. Hematopoietic stem cell fate is established by the Notch–Runx pathway. Genes & Development. 2005; 19:2331–2342. [PubMed: 16166372]
37. Garg V, et al. Mutations in NOTCH1 cause aortic valve disease. Nature. 2005; 437:270–274. [PubMed: 16025100]
38. Taniuchi I, Littman DR. Epigenetic gene silencing by Runx proteins. Oncogene. 2004; 23:4341–4345. [PubMed: 15156191]
39. Weng AP, et al. Growth suppression of pre-T acute lymphoblastic leukemia cells by inhibition of notch signaling. Mol Cell Biol. 2003; 23:655–664. [PubMed: 12509463]
40. Isakov N, Altman A. PROTEIN KINASE Cθ IN T CELL ACTIVATION. Annual Review of Immunology. 2002; 20:761–794.

References for Online Methods

41. Morita S, Kojima T, Kitamura T. Plat-E: an efficient and stable system for transient packaging of retroviruses. Gene Ther. 2000; 7:1063–1066. [PubMed: 10871756]
42. Zufferey R, Nagy D, Mandel RJ, Naldini L, Trono D. Multiply attenuated lentiviral vector achieves efficient gene delivery in vivo. Nat Biotech. 1997; 15:871–875.
43. Dull T, et al. A Third-Generation Lentivirus Vector with a Conditional Packaging System. Journal of Virology. 1998; 72:8463–8471. [PubMed: 9765382]
44. Zufferey R, et al. Self-Inactivating Lentivirus Vector for Safe and Efficient In Vivo Gene Delivery. Journal of Virology. 1998; 72:9873–9880. [PubMed: 9811723]
45. Zennou V, et al. HIV-1 Genome Nuclear Import Is Mediated by a Central DNA Flap. Cell. 2000; 101:173–185. [PubMed: 10786833]
46. Sirven A, et al. The human immunodeficiency virus type-1 central DNA flap is a crucial determinant for lentiviral vector nuclear import and gene transduction of human hematopoietic stem cells. Blood. 2000; 96:4103–4110. [PubMed: 11110680]
47. Logan AC, et al. Factors influencing the titer and infectivity of lentiviral vectors. Hum Gene Ther. 2004; 15:976–988. [PubMed: 15585113]

48. Robbins PB, et al. Consistent, persistent expression from modified retroviral vectors in murine hematopoietic stem cells. PNAS. 1998; 95:10182–10187. [PubMed: 9707621]

49. Root DE, Hacohen N, Hahn WC, Lander ES, Sabatini DM. Genome-scale loss-of-function screening with a lentiviral RNAi library. Nat Meth. 2006; 3:715–719.

50. Ou, Wb; Zhu, Mj; Demetri, GD.; Fletcher, CDM.; Fletcher, JA. Protein kinase C- [theta] regulates KIT expression and proliferation in gastrointestinal stromal tumors. Oncogene. 2008; 27:5624–5634. [PubMed: 18521081]

51. Sarbassov DD, Guertin DA, Ali SM, Sabatini DM. Phosphorylation and Regulation of Akt/PKB by the Rictor-mTOR Complex. Science. 2005; 307:1098–1101. [PubMed: 15718470]

52. Palomero T, et al. Mutational loss of PTEN induces resistance to NOTCH1 inhibition in T-cell leukemia. Nat Med. 2007; 13:1203–1210. [PubMed: 17873882]

53. Dallas MH, Varnum-Finney B, Martin PJ, Bernstein ID. Enhanced T-cell reconstitution by hematopoietic progenitors expanded ex vivo using the Notch ligand Delta1. Blood. 2007; 109:3579–3587. [PubMed: 17213287]

54. Schneider CA, Rasband WS, Eliceiri KW. NIH Image to ImageJ: 25 years of image analysis. Nat Meth. 2012; 9:671–675.

55. Aster JC, et al. Oncogenic forms of NOTCH1 lacking either the primary binding site for RBP-Jkappa or nuclear localization sequences retain the ability to associate with RBP-Jkappa and activate transcription. J. Biol. Chem. 1997; 272:11336–11343. [PubMed: 9111040]

56. Ji H, et al. An integrated software system for analyzing ChIP-chip and ChIP-seq data. Nat Biotech. 2008; 26:1293–1300.

57. Schadt EE, Li C, Ellis B, Wong WH. Feature extraction and normalization algorithms for high-density oligonucleotide gene expression array data. J Cell Biochem Suppl. 2001; (Suppl 37):120–125. [PubMed: 11842437]

58. Hu Y, Smyth GK. ELDA: Extreme limiting dilution analysis for comparing depleted and enriched populations in stem cell and other assays. Journal of Immunological Methods. 2009; 347:70–78. [PubMed: 19567251]

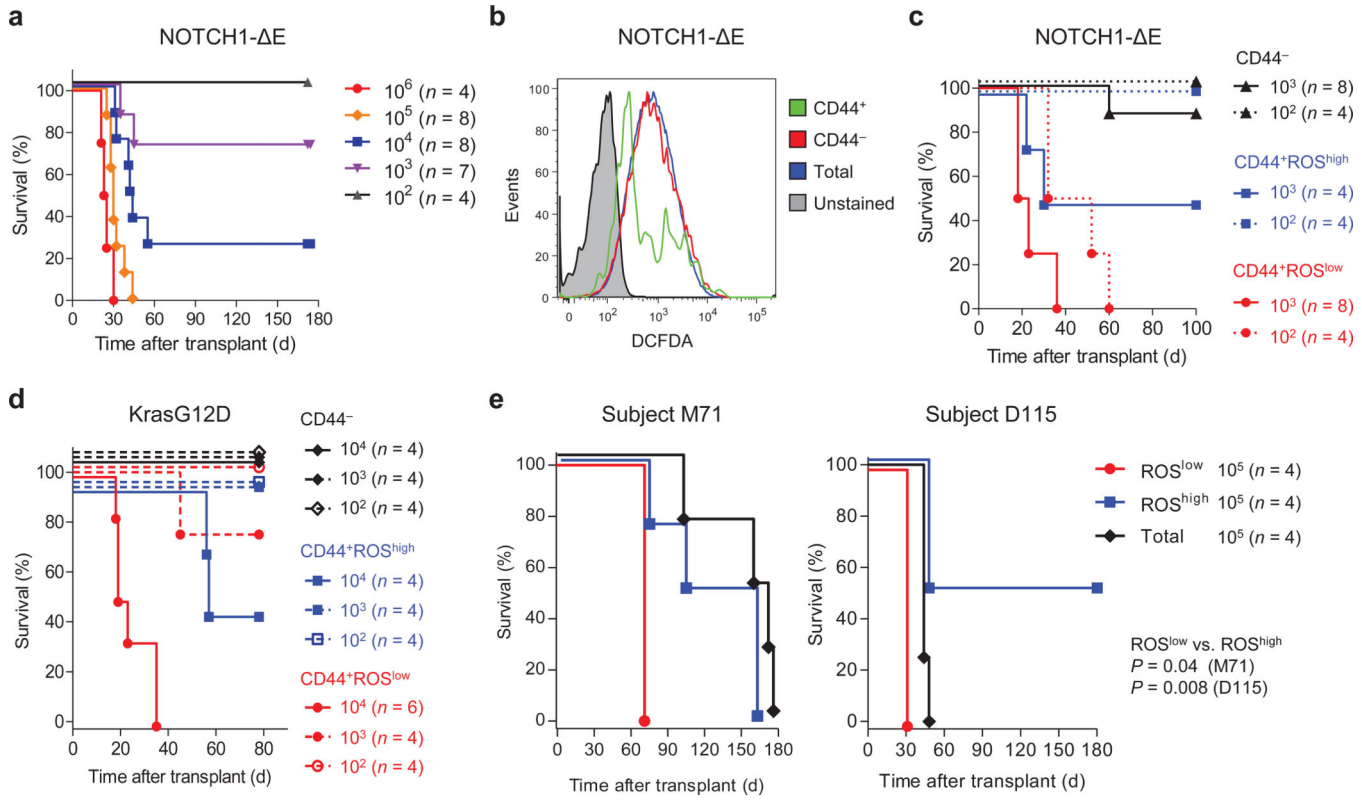

Figure 1. Leukemia-initiating cells (LICs) in T-ALL are characterized by low ROS

(**a,c,d,e**) Survival of recipient mice following transplantation with primary mouse (**a,c**) NOTCH1-ΔE or (**d**) K-ras^{G12D} leukemias, or (**e**) xenograft-expanded primary human T-lymphoblasts. Either (**a**) total leukemia cells or (**c–e**) FACS-sorted subsets were injected by tail vein into (**a,c,d**) syngeneic C57BL/6 or (**e**) immunodeficient NSG recipients. The number of cells injected per mouse and number of mice injected for each cellular subset are as indicated. The calculated LIC frequency in **a** is 1 in ~6,000 cells (95% CI of 1 in 2,800–13,200 cells). Statistical significance in **e** was calculated by Log-rank test. Raw survival data for all transplant experiments are summarized in Supplementary Table 1.

(**b**) Flow cytometric analysis of reactive oxygen species (ROS) levels by DCFDA staining in CD44^{+} and CD44^{-} subsets or total cells from a primary mouse NOTCH1-ΔE leukemia. Data depicted are representative of multiple replicates.

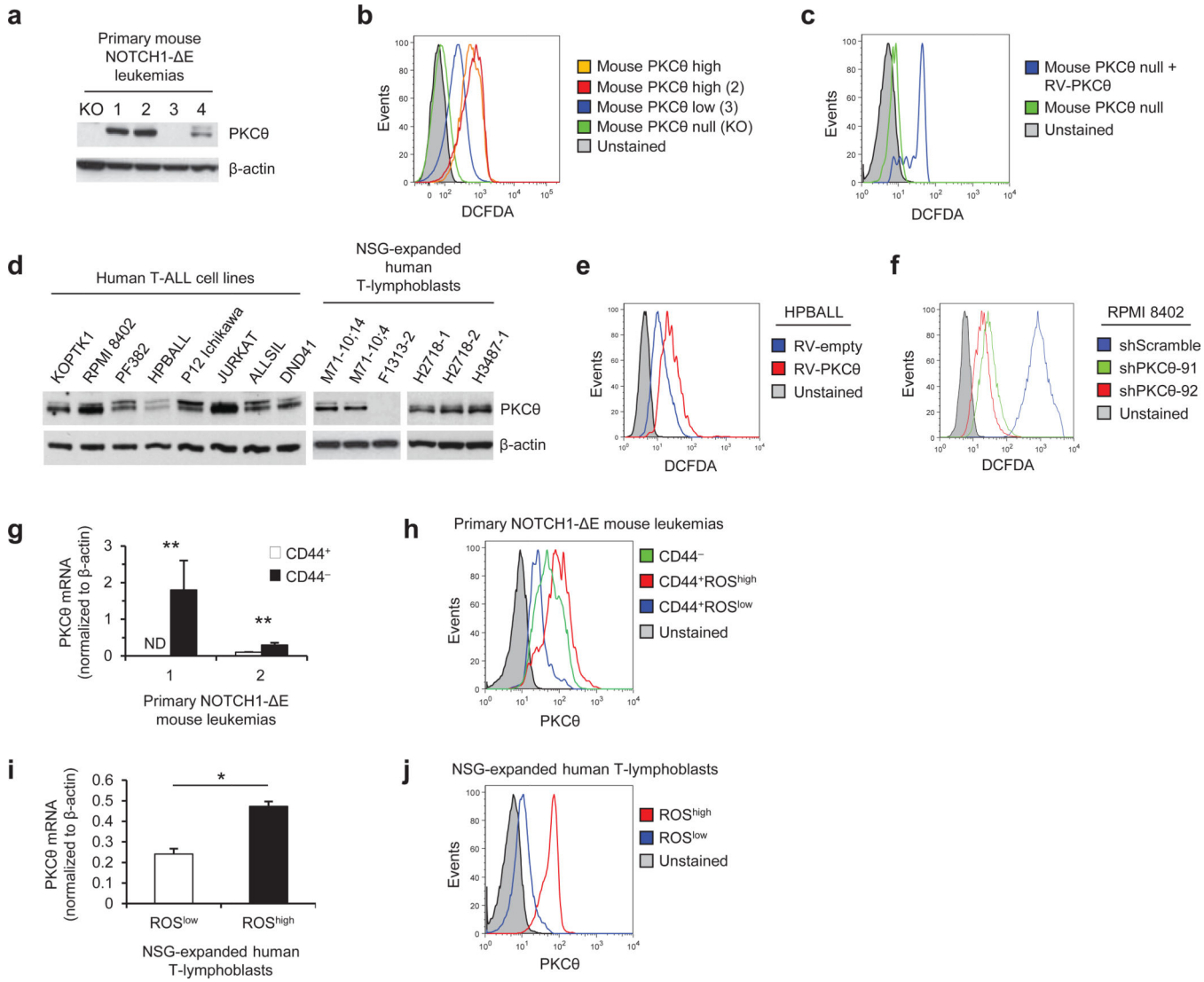

Figure 2. PKCθ dictates ROS levels and is asymmetrically distributed to LIC-depleted cell fractions

(**a**) Western blot analysis of PKCθ protein expression in primary mouse NOTCH1-ΔE leukemias from wild-type (samples 1–4) and PKCθ^{null} (KO) backgrounds.

(**b,c**) Flow cytometric analysis of intracellular ROS levels by DCFDA staining in mouse NOTCH1-ΔE leukemias with naturally varying (high vs. low) and engineered levels of PKCθ expression (PKCθ^{null}, knocked-out by genetic deletion; RV-PKCθ, enforced by retroviral transduction).

(**d**) Western blot analysis of PKCθ protein expression in human T-ALL cell lines and primary human T-lymphoblasts following expansion as xenografts in NSG mice (The two samples for each of M71 and H2718 represent different mice engrafted with the same human sample).

(**e,f**) Flow cytometric analysis of intracellular ROS levels by DCFDA staining in human T-ALL cell lines with engineered levels of PKCθ expression (RV-PKCθ, enforced by

retroviral transduction; RV-empty, empty retrovirus control; shPKCθ-2 and -3, knocked-down by two different lentiviral shRNAs; shScramble, scrambled shRNA negative control). (**g–j**) Analysis of PKCθ expression in FACS-sorted LIC-enriched ($CD44^{+}$, ROS^{low}) vs. LIC-depleted ($CD44^{-}$, ROS^{high}) subsets from freshly explanted (**g,h**) mouse NOTCH1-ΔE leukemias and (**i,j**) xenograft-expanded primary human T-ALLs. (**g,i**) Quantitative RT-PCR analysis of PKCθ mRNA levels. Error bars indicate standard deviation. (**h,j**) Flow cytometric analysis of PKCθ protein expression.

All data depicted in this figure are representative of multiple replicates. *, $P<0.05$; **, $P<0.01$; ***, $P<0.001$ (*Student's t-test*); *ND, not detected*.

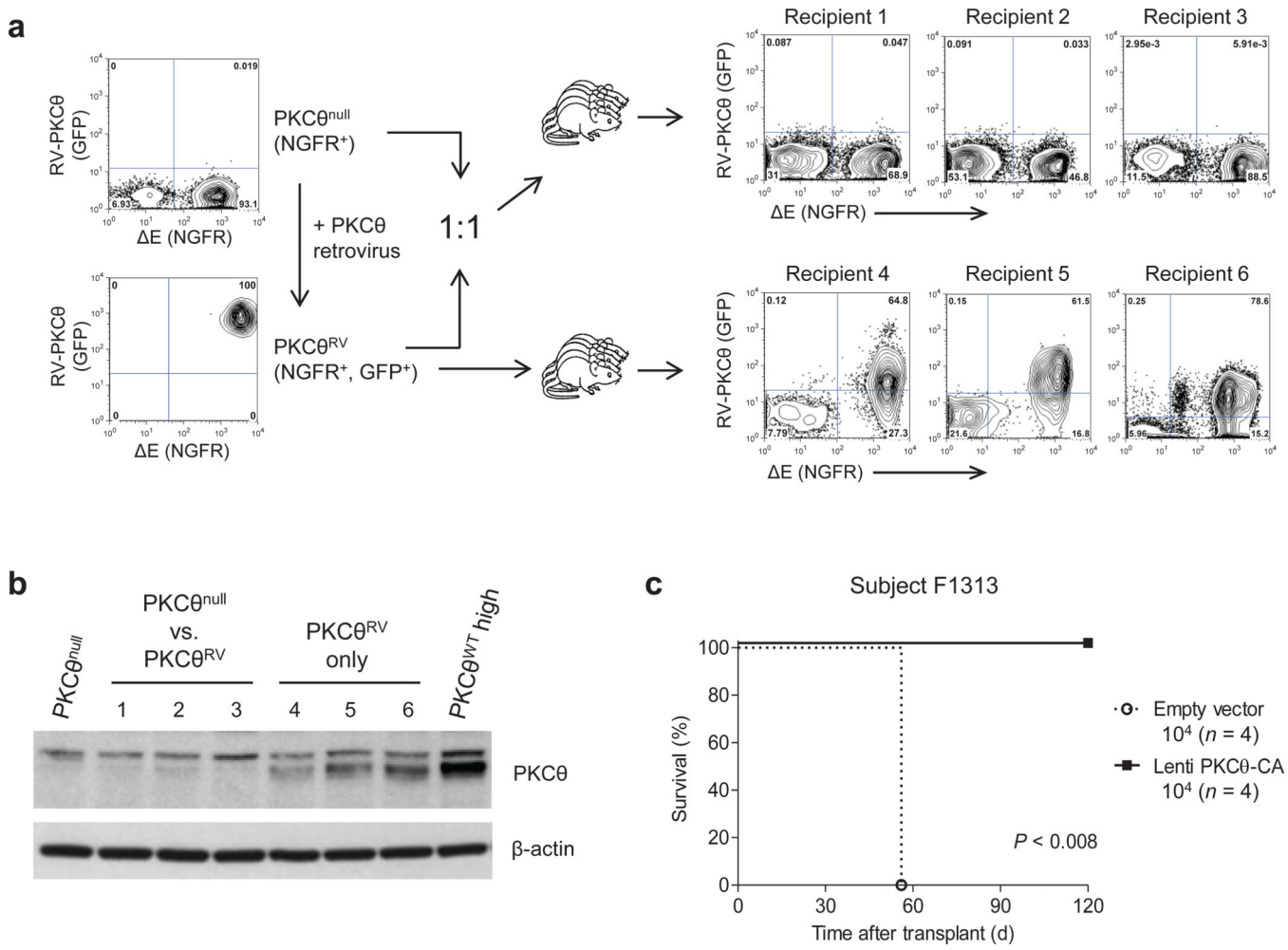

Figure 3. Increased PKCθ expression compromises disease reconstitution *in vivo*

(**a**) Competitive transplant assay between PKCθ^{null} and PKCθ^{RV} NOTCH1-ΔE leukemia cells (upper arm, recipients 1–3) and non-competitive transplant of PKCθ^{RV} cells (lower arm, recipients 4–6). 1×10^4 PKCθ^{null} leukemia cells plus 1×10^4 PKCθ^{RV} cells (PKCθ^{null} leukemia cells transduced with PKCθ retrovirus), or 1×10^4 PKCθ^{RV} cells only were i.v. injected into syngeneic C57BL/6 recipient mice (n = 4). All animals developed aggressive leukemia within 3 weeks. Moribund mice were euthanized and bone marrow or spleen analyzed by flow cytometry for PKCθ^{null} (NGFR$^+$GFP$^-$) vs. PKCθ^{RV} (NGFR$^+$GFP$^+$) leukemia cell content. Data depicted are representative of two replicate experiments.

(**b**) Western blot analysis for PKCθ protein expression in leukemias arising from competitive (recipients 1–3) and non-competitive (recipients 4–6) transplant assays as depicted in **a**.

(**c**) Survival of mice transplanted with human T-ALL cells which had been transduced with constitutively activated PKCθ lentivirus. T-lymphoblasts from a xenograft-expanded human sample with very low/non-detectable levels of endogenous PKCθ expression (F1313-2; see western blot in Fig. 2d) were transduced with lentivirus encoding a constitutively activated form of PKCθ (A148E; PKCθ-CA) or empty vector and FACS sorted for the viral GFP marker. 1×10^4 sorted GFP$^+$ cells were injected into each of four immunodeficient NSG

recipient mice. Animals were monitored daily for development of leukemia; moribund animals were euthanized and disease confirmed at necropsy. Significance *P*-value was calculated by Log-rank test.

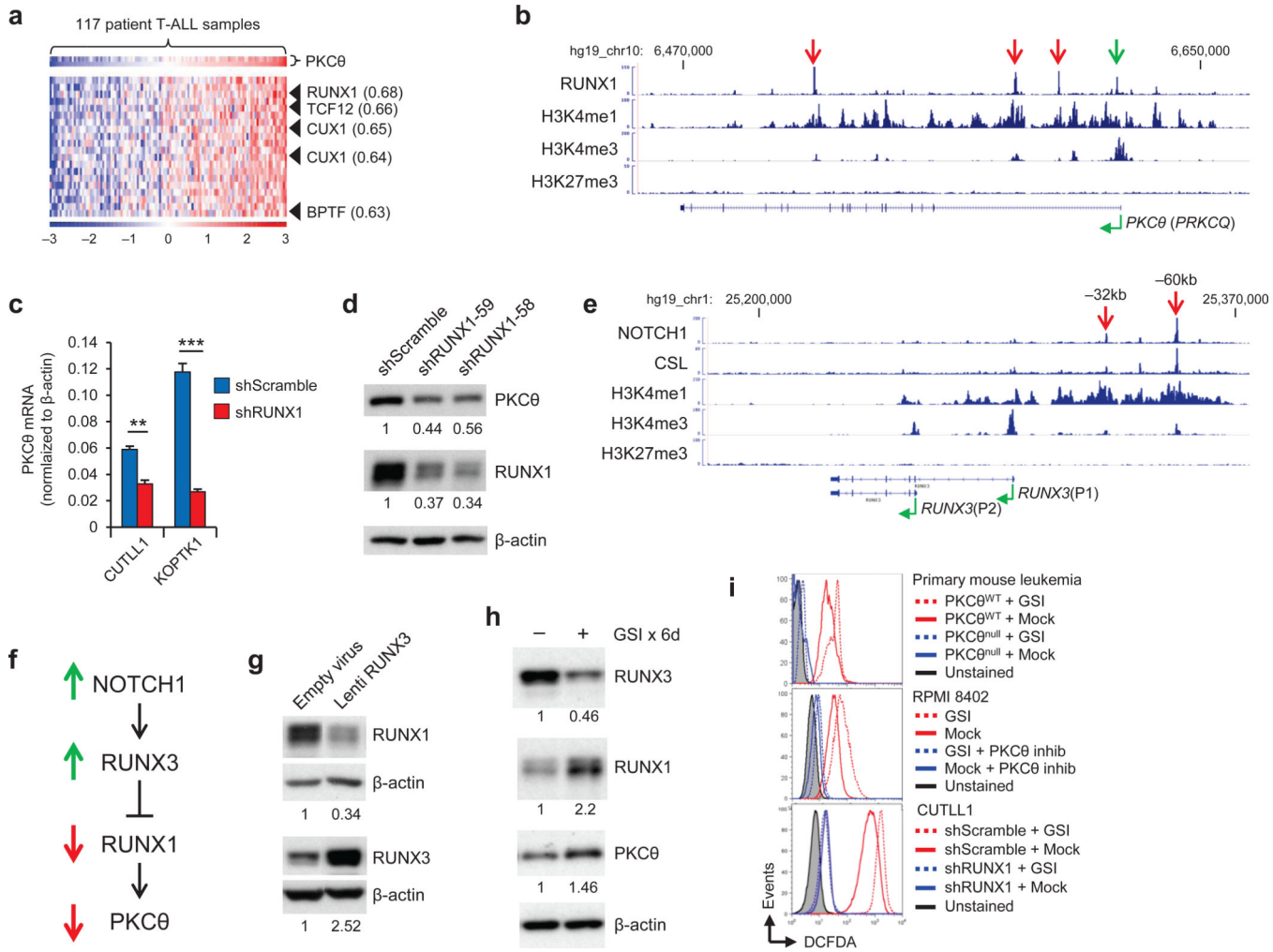

Figure 4. NOTCH1 represses PKCθ and ROS via RUNX3 and RUNX1

(**a**) Microarray expression profile data from primary human T-ALL samples (GSE26713). Samples are ordered left-to-right by PKCθ expression level. Top 20 genes most correlated with PKCθ are ordered top-to-bottom. Identified transcription factors are indicated with Pearson's correlation coefficient (*r*) in parentheses. Expression levels are normalized for each probeset across all samples with mean = 0 and standard deviation = 1.

(**b,e**) ChIP-Seq reads for the indicated antibodies over human (**b**) PKCθ and (**e**) RUNX3 loci from the human T-ALL cell line CUTLL1. Promoters (green arrows) and putative enhancers (red arrows) are indicated.

(**c**) Quantitative RT-PCR analysis of PKCθ mRNA levels in human T-ALL cell lines transduced with lentiviral shRNAs against RUNX1 or scrambled negative control (shScramble). Error bars indicate standard deviation for assays performed in triplicate. **, $P<0.01$; ***, $P<0.001$ (*Student's t-test*).

(**d,g,h**) Western blot analyses of PKCθ, RUNX1, and RUNX3 protein levels in CUTLL1 cells following (**d**) shRNA-mediated knock-down of RUNX1, (**g**) lentiviral overexpression of RUNX3, and (**h**) Notch inhibition with γ-secretase inhibitor (GSI, 1 μM compound E).

Numbers below each panel indicate fold change after normalization to β-actin loading control.

(**f**) Schematic of transcriptional circuit involving NOTCH1, RUNX3, RUNX1, and PKCθ.

(**i**) Flow cytometric analysis of intracellular ROS levels by DCFDA staining in T-ALL cells treated with GSI, myristoylated PKCθ pseudosubstrate inhibitor, and/or transduced with RUNX1 shRNAs. Cells were treated with GSI for 3 days with PKCθ inhibitor added in the final 24 hours before assay. Gated live events are shown. Data depicted are representative of multiple replicates.